Applied Thermal Engineering 254 (2024) 123883

Contents lists available at ScienceDirect

Applied Thermal Engineering

journal homepage: www.elsevier.com/locate/ate

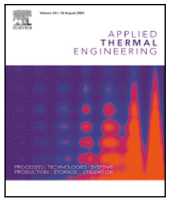

Research Paper

Effects of simultaneous soft faults in a reversible and variable-speed air-to-water heat pump

Belén Llopis-Mengual *, Emilio Navarro-Peris

Instituto Universitario de Investigación de Ingeniería Energética (IUIIE), Universitat Politècnica de València (UPV), Camino de Vera s/n, 46022 Valencia, Spain

ARTICLE INFO

Keywords:
Air-to-water heat pump
Soft fault
Variable-speed compressor
Subcooling control
R290
Fault detection and diagnosis

ABSTRACT

The widespread adoption of air-to-water heat pumps is driven by their high heating efficiency, with some systems offering reversibility for cooling applications. Despite their benefits, these systems are susceptible to soft faults such as undercharge, overcharge, and outdoor unit airflow restrictions (condenser fouling in cooling mode or evaporator fouling in heating mode). Detecting and addressing these faults before they escalate into hard faults is critical. While previous experimental studies have focused on residential heat pumps with imposed faults, most were conducted on air-to-air systems, primarily in cooling mode and with fixed-speed compressors. This study addresses the gap by investigating a reversible air-to-water heat pump employing R290 and a variable-speed compressor. The experimental work consists of imposing faults of undercharge, overcharge, condenser and evaporator fouling, individually and in combination. The investigation analysis considers the system's behavior under these faults in cooling and heating modes and how the control strategy (subcooling or superheat) and a compressor suction accumulator affect it. In cooling mode, the combination of 85% undercharge and 50% condenser fouling worsens the EER up to 39% if the superheat is controlled and up to 10% if the subcooling is controlled. In heating mode with subcooling control, 85% undercharge combined with a 50% evaporator fouling can worsen the COP by 32%. However, there are cases where those same fault levels only impact the COP by 4% due to the charge requirements of the condition and that the excess charge is stored in the compressor suction accumulator. As compressor speed can significantly affect the refrigerant charge requirements of the system, this work shows its potential for fault detection, particularly for undercharge. These findings can provide a basis for developing Fault Detection and Diagnosis methodologies for reversible air-to-water heat pumps with variable-speed compressors.

1. Introduction

In 2021, a significant 64.4% of the final energy consumption in the European Union (EU) residential sector was dedicated to home heating. An additional 14.5% of energy consumption was attributed to water heating [1]. In response to the pressing need for sustainable and energy-efficient heating solutions, heat pumps (HP) have emerged as a promising alternative to traditional methods. The European Heat Pump Association (EHPA) reports that heat pump sales increased by 39% in 2022, marking the highest annual growth rate since 2010 [2].

Nevertheless, HPs are complex systems and are susceptible to operating under soft fault conditions that can lead them to not reach their optimal performance levels. Common examples of these soft faults, often addressed in the literature [3] include improper refrigerant charge levels in the system, either overcharge (OC) due to installation errors or undercharge (UC) due to system leaks. Other prevalent faults are fouling in the external heat exchanger, caused by the accumulation of leaves or dirt that reduce efficiency. Depending on the mode of operation in an air-to-water heat pump (cooling or heating), this fault will result in condenser fouling (CF) or evaporator fouling (EF), respectively. These faults can lead to reduced heating or cooling capacity and increased energy consumption. If undetected, soft faults may significantly affect both actual and seasonal performance in heating and cooling modes. Simulation studies, such as those by [4], have shown that a 30% undercharge of refrigerant can increase energy use by approximately 20%, regardless of the climate. Similarly, [5] investigated performance degradation using a physics-based model, concluding that SCOP is penalized by 13% for a maximum CF of 40%, 2% for a maximum EF of 40%, and 25% for a 10% per year refrigerant leakage. In cooling mode, corresponding penalizations are 14%, 13%, and 41% for the same fault intensity levels. The work developed in [6] experimentally tested a reversible heat pump with induced faults

* Corresponding author.
E-mail address: belen.llopis@iie.upv.es (B. Llopis-Mengual).

https://doi.org/10.1016/j.applthermaleng.2024.123883
Received 17 March 2024; Received in revised form 5 June 2024; Accepted 3 July 2024
Available online 8 July 2024

Nomenclature

Acronyms

BPHX	Brazed Plate Heat Exchanger
CF	Condenser Fouling
CHEX	Finned-tube (coil) Heat Exchanger
Comp.	Compressor
EEV	Electronic Expansion Valve
EF	Evaporator Fouling
EU	European Union
FDD	Fault Detection and Diagnosis
OC	Overcharge
UC	Undercharge

Variables

ΔP	Pressure drop (Pa)
$\dot{m}_{ref}$	Refrigerant mass flow rate (kg/h)
$\dot{m}_{water}$	Water mass flow rate (kg/h)
W_{comp}	Compressor power input (kW)
W_{fan}	Fan power input (kW)
W_{total}	Total power input (kW)
A	Inlet air dry bulb temperature (°C)
COP	Coefficient of Performance (–)
EER	Energy Efficiency Ratio (–)
fc	Compressor speed (rps)
Qcond	Condenser (heating) capacity (kW)
Qevap	Evaporator (cooling) capacity (kW)
R(X)	Residual of variable X (Units of X, except for X = COP/EER or X = Qcond/Qevap, that units are (%))
RH	Relative Humidity (%)
SC	Subcooling (K)
SH	Superheat (K)
Tc	Condensing temperature (°C)
Tdis	Compressor discharge temperature (°C)
Te	Evaporating temperature (°C)
W	Outlet water temperature (°C)

to assess seasonal performance under improper airflow and refrigerant charge conditions. The study found that combined decreases in airflow and refrigerant charge could reduce the unit's heating seasonal COP by 10%.

In order to develop Fault Detection and Diagnosis (FDD) methodologies, numerous studies have been conducted by inducing faults in heat pumps within laboratory conditions to investigate their performance when such faults occur. This research has predominantly focused on air-to-air systems for residential air conditioning, particularly in the United States, where this system type is most common. For instance, [7] examined the effects of UC/OC, EF, and CF on system capacity and Coefficient of Performance (COP) in various air-to-air systems. Studies like [8,9] utilized numerous experimental tests with heat pumps to systematically investigate the generalized effects of different types of faults on system variables. [10] investigated the performance of virtual sensors by imposing double faults on a rooftop unit (RTU) and a direct expansion split system; however, they did not present the results regarding the impact of these double faults. [11] investigated the performance degradation of a residential heat pump in heating mode under single fault conditions, highlighting significant impacts from faults like OC, EF, and CF. Additionally, [12,13], and [14] introduced soft faults to an air-to-air heat pump operating in cooling mode, both individually and in combination, to study performance degradation.

While extensive research exists on air-to-air units, most studies focus on units with fixed-speed compressors. With the increasing use of variable-speed heat pumps, which adapt compressor speed to demand, performance differences under soft fault conditions become significant. For example, [15] tested a variable-speed water-to-water system and found reduced sensitivity to faults due to the compressor speed control mechanism. [16] described the effects of soft faults in a variable-speed water-to-water heat pump using R290 in heating mode. Moreover, [17] described a data mining-based FDD for a variable-speed air-to-water heat pump in heating mode, without detailing fault effects. [18] tested an air-to-water prototype with a variable-speed compressor under EF and refrigerant charge faults; these faults were imposed individually and exclusively during heating mode.

A noticeable research gap exists in the experimental investigation of residential air-to-water heat pumps under both individual and simultaneous soft fault conditions, especially across both cooling and heating modes. With UC and OC faults in this system typology, it is crucial to know how the unit performs in case of higher or lower charge levels than the nominal one. When switching from cooling to heating modes, the refrigerant charge needs and the difference in internal volume between heat exchangers can cause distinct effects. [19] conducted an experimental analysis of the refrigerant mass distribution of various cycle components in a reversible air-to-water heat pump utilizing R32. The findings highlighted notable differences in the distribution of refrigerant charge based on the conditions and mode.

Addressing this issue, some studies, like [20], suggest using a receiver in the compressor suction and subcooling control to compensate for charge variations, ensuring saturation conditions at the evaporator outlet. Consequently, heat pump circuits with a receiver at the evaporator outlet and subcooling control are emerging, showing higher performance [21,22]. [23] evaluated optimal subcooling to improve heat pump's performance and [24] explored different subcooling control strategies to reach maximum efficiency. However, no experimental studies have investigated this circuit typology with subcooling control under soft fault conditions.

This study addresses these gaps by examining the effects of UC, OC, EF, and CF (both individually and simultaneously) in a residential air-to-water heat pump with a variable-speed compressor using R290 as a refrigerant. The experimental setup includes an accumulator at the evaporator outlet, operating with subcooling or superheating control based on the mode. This research explores how controllable external parameters, such as compressor speed, influence system performance under these faults. Additionally, it investigates distinct effects on variables and performance impacts during cooling and heating modes, providing insights for FDD development in this heat pump typology.

2. Methodology

2.1. Experimental setup

The experimental unit investigated in this study is a reversible air-to-water heat pump with 7 kW of nominal capacity, utilizing R290 (propane) as the refrigerant. Fig. 1 shows the diagram of the experimental setup with the primary components of this heat pump, which include a variable-speed rotary compressor, a brazed plate heat exchanger (BPHX), a finned-tube (coil) heat exchanger (CHEX), an electronic expansion valve (EEV), a 4-way reversible valve and a compressor suction accumulator.

The unit is tested in a psychrometric chamber capable of recreating the needed working conditions of the heat pump. Fig. 1 provides a schematic representation of the tested heat pump, including its components and the sensor locations within the system. These sensors include the compressor suction and discharge pressure, refrigerant temperature before and after each component, as well as water and air temperature.

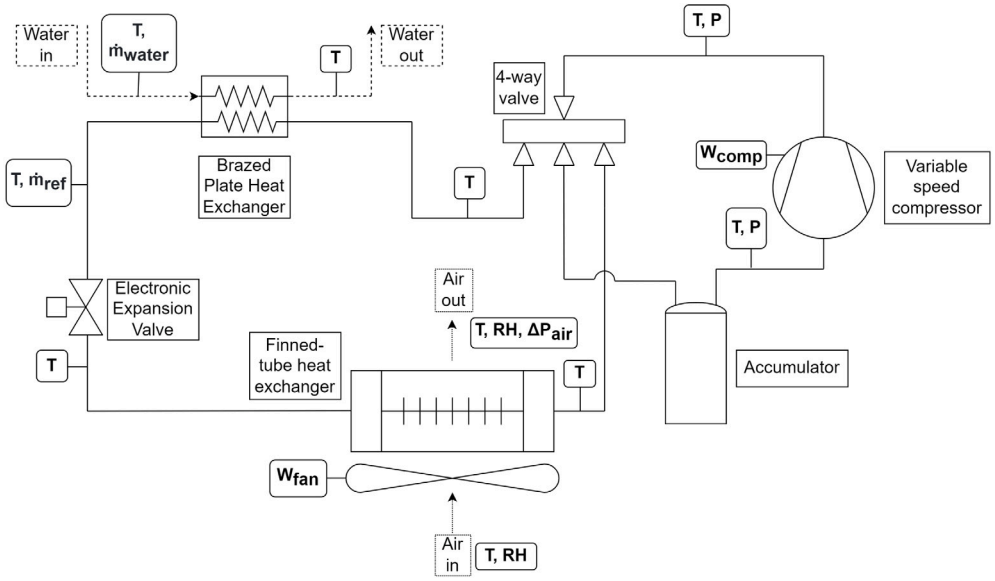

Fig. 1. System diagram of the experimental setup.

Table 1
Measurement instruments used in the experimental campaign and their range and total error.

Measurement	Instrument	Range	Total error
Refrigerant temperature	Thermocouple type T	−270–400 °C	±0.8 (°C)
Water and air temperature	Thermoresistance PT-100	−220–850 °C	±0.07 (°C)
Suction and discharge pressure	Pressure transducer Rosemount 3051	0–15 bar (suction) 10-45 bar (discharge)	±0.06 (bar)
Refrigerant mass flow rate	Coriolis flowmeter Micro Motion CMFS015M	0–5600 kg/h	±0.13 (kg/h)
Water mass flow rate	Coriolis flowmeter Mass 2100	0–245 kg/h	±4.48 (kg/h)
Air relative humidity	Vaisala Humicap 180	0%–100%	±2.77 (%)
Pressure drop in the finned-tube HX	Differential pressure transducer DPT-4001	0–25 Pa	±0.2 (Pa)
Total power input			±0.0144 (kW)
Fan power input	Power meter A2000 Gossen Metrawatt	0–2.5 kW (configured)	±0.0102 (kW)
Compressor power input			±0.0139 (kW)

To determine the refrigerant mass flow rate in heating mode, a Coriolis flowmeter is installed at the outlet of the BPHX. As the water flow rate is measured with another Coriolis flowmeter, the refrigerant flow rate in cooling mode is obtained with the balance in the BPHX. The fan's airflow is determined using an averaging pitot tube flowmeter. The refrigerant charge used in each test is measured using a Gram LHK-150 scale, which has a 10 g resolution. Further details on the instruments used, including their range and total error derived from the uncertainty analysis, are provided in Table 1.

Since this heat pump is reversible, it operates in two distinct modes (cooling and heating), each governed by a specific control strategy:

Cooling mode:

In cooling mode, the BPHX functions as the evaporator to cool the water. The heat pump employs two control strategies:

- **Superheat (SH) Control:** The expansion valve regulates the SH at the compressor suction, a common practice in systems based in vapor compression cycles. This will be the case under most operating conditions for cooling mode. Although the system includes an accumulator at the compressor suction, maintaining a controlled SH means that the accumulator remains nearly empty. Most of the refrigerant charge is concentrated in the condenser in a liquid state, which varies as the required refrigerant charge changes by varying operating conditions.
- **Subcooling (SC) Control:** When the water outlet temperature is below 7 °C, the EEV switches to maintain a SC of 2–3 K. This prevents the evaporating temperature from dropping below 0 °C, thus avoiding the risk of evaporator freezing.

Heating mode:

In heating mode, the BPHX serves as the condenser for heating water. The heat pump tested in this study is optimized for heating mode, so this will be its main mode of operation. Here, the control strategy is to maintain subcooling:

- **Subcooling (SC) Control:** The EEV regulates the SC at the condenser outlet to a target value of 6–10 K, optimized for the specific operating conditions. The accumulator at the compressor suction stores the excess refrigerant, ensuring saturation conditions at the evaporator outlet and operating with minimal or zero superheat.

The accumulator serves as a reservoir for refrigerant charge at the compressor suction when SC control is used. Depending on operational conditions, a specific amount of refrigerant is needed to function, with the rest stored in the accumulator. Though physically present in the system, this stored refrigerant remains effectively separated during operation.

2.2. Test campaign

The experimental campaign has been conducted in both cooling and heating modes. Operating conditions representative of typical system operation have been selected. In the cooling mode, three different operating conditions have been tested, which can be seen in Table 2. This table shows the air inlet, water inlet and outlet temperature, and the compressor speed. Likewise, four different conditions have been tested in the heating mode, as shown in Table 3. Notably, frost generation

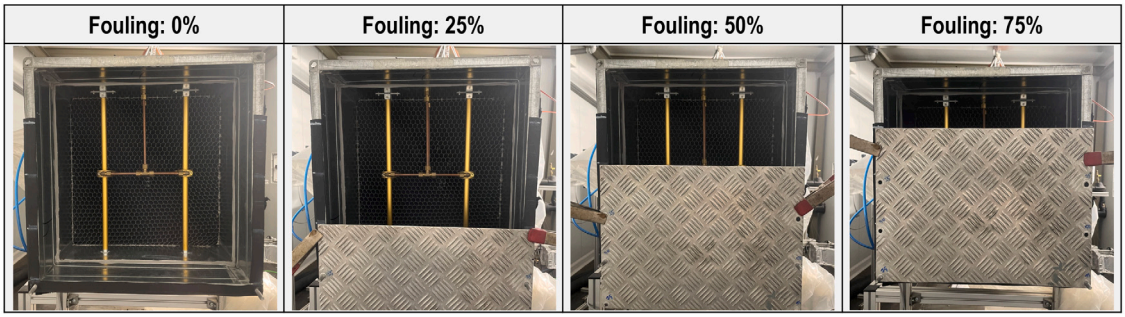

Fig. 2. Imposed fouling or airflow restriction at the air outlet.

Table 2
Experimental test conditions in cooling mode.

Test condition	Inlet air dry bulb T (°C)	Inlet water T (°C)	Outlet water T (°C)	Comp. speed (rps)
A23W18-80rps	23	23	18	80
A35W7-30rps	35	12	7	30
A35W18-60rps	35	23	18	60

Table 3
Experimental test conditions in heating mode.

Test condition	Inlet air dry bulb T (°C)	Inlet water T (°C)	Outlet water T (°C)	Comp. speed (rps)
A10W45-80rps	10	38	45	80
A12W24-40rps	12	20	24	40
A2W35-35rps	2	32	35	35
A7W70-80rps	7	64	70	80

Table 4
Imposed fault levels in both modes.

Fault	Imposed fault levels (%)
Refrigerant charge	85, 100, 110
Fouling	0, 25, 50, 75

Table 5
Number of experimental tests performed by type of fault or combination of faults.

Fault(s)	Cooling	Heating
UC	3	4
OC	3	4
Fouling[a]	9	12
UC+Fouling[a]	9	12
OC+Fouling[a]	9	12
Fault-free	3	4
Total number of tests in each mode	36	48
Total number of tests	84	

[a] Fouling refers to CF in cooling mode and EF in heating mode.

was absent in these examined conditions, making defrosting measures unnecessary. Consequently, this factor has not been incorporated into the scope of this study.

The faults imposed in all tested conditions are undercharge (UC), overcharge (OC), and outdoor unit fouling. The selection of these specific faults is based on the recognition that both UC and fouling can manifest over time due to leaks or the accumulation of dirt and debris on the external heat exchanger, respectively. Another potential fault that this study does not consider is the presence of non-condensable gases, which may result from installation errors and could manifest in the unit's performance shortly after installation, so it has not been included. The overcharge (OC) fault, while also originating from installation errors, is deliberately introduced in this study to assess the unit's performance under different charge levels and to observe its response to being charged beyond the manufacturer's recommended specifications due to the specific typology and control method of the tested unit. According to the manufacturer's indications, the unit has a nominal charge of 0.95 kg of R290. Thus, the UC has been imposed with 85% of this nominal charge, and the OC fault has been implemented with a refrigerant charge level of 110%.

The imposed outdoor unit fouling fault simulates a blockage in the air heat exchanger due to dirt or other elements deposited on the fan or coil. The main effect of this fault is a pressure drop that reduces the fan's airflow rate. Depending on the working mode, this fault would be Condenser Fouling (CF) in cooling and Evaporator Fouling (EF) in heating. In these experimental tests, this fault has been imposed by obstructing the air outlet to artificially generate the expected pressure drop. The fault is defined as the percentage of surface area blocked, as shown in the pictures in Fig. 2.

These faults have been tested experimentally, both individually and combined. Table 4 shows a summary of the faults and their imposed levels, and Table 5 the number of tests carried out in the experimental campaign by working mode and fault or combination of faults.

The experimental values measured in the unit are presented in the form of residuals for each variable ($R(X)$), which are the difference between the studied variable in fault conditions (X_{faulty}) and the same variable at the same conditions but fault-free ($X_{fault-free}$), following Eq. (1).

$$R(X) = X_{faulty} - X_{fault-free} \tag{1}$$

2.3. Heat pump model

In addition to the experimental investigations, this study employed a heat pump model utilizing IMST-ART [25]. This software for simulating vapor compression cycles uses submodels of each component, whose global model is formed by a system of nonlinear equations solved with a Newton–Raphson solver. The compressor submodel uses its geometrical data, the oil (solubility, circulation rate), heat losses, and the cooling capacity and power input catalog data for different compressor speeds. It interpolates according to the indicated conditions to obtain the volumetric and compressor efficiency to calculate the rest of the cycle. Heat exchanger models use detailed geometry, employing the SEWTLE solution method [26] through discretization into cells along refrigerant and secondary fluid paths. In addition, the model uses REFPROP [27] for the calculation of the properties of the refrigerant. The model's robustness has been established through validation against experimental data under steady-state conditions in numerous studies (like [28–30]) with prediction errors ranging from 5% and 10% of the Maximum Relative Error. In [31], it describes in detail how the overall model of the heat pump, heat exchangers, compressor, connections, and expansion devices are made, as well as the calculation of the solution. Further details on the model are also available in [32], which explains how the modeling is performed in IMST-ART for fault-free and faulty

Table 6
Refrigerant charge required at each tested operating point of the cooling mode (calculated with the model).

Test condition	Water inlet T (°C)	Water outlet T (°C)	Condenser inlet T (°C) and RH (%)	Airflow (m3/h)	Compressor speed (rps)	SC (K)	SH (K)	Required charge (kg)
A23W18-80rps	23	18	23 (82%)	1900	80	14.5	5	0.72
A35W7-30rps	12	7	35 (72%)	1900	30	2.0	0	0.54
A35W18-60rps	23	18	35 (76%)	1900	60	10.5	7	0.68

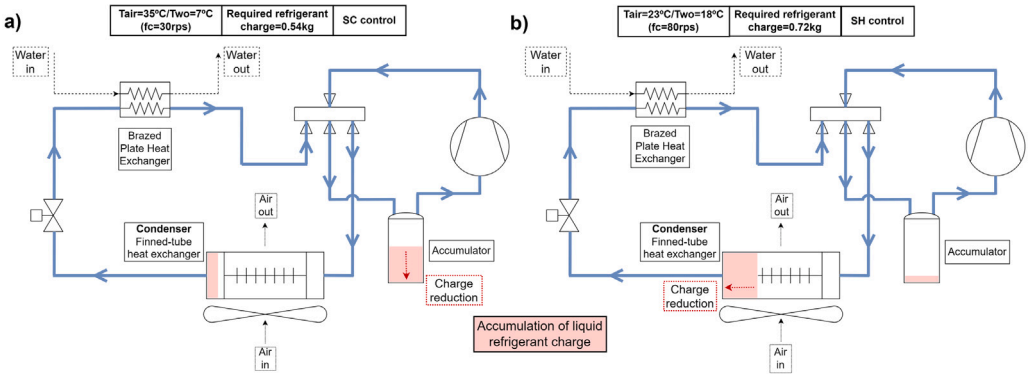

Fig. 3. Schematic diagram illustrating the liquid refrigerant charge accumulation and where it is reduced in case of undercharge in cooling mode for conditions (a) A35W7-30rps and (b) A23W18-80rps.

conditions, single and simultaneous, for a given heat pump. In the present study, the generated model has been used to calculate, according to the conditions, the refrigerant charge required by the system. Therefore, the refrigerant charge of the cycle is calculated using the subcooling as input of the model previously described (geometry of the components, heat transfer and pressure drop correlations, void fraction correlations for the two-phase zones). The calculated refrigerant charge with the model serves as a guide for estimating the required amount under specific conditions.

3. Results and discussion

3.1. Refrigerant undercharge/overcharge

3.1.1. Cooling mode

To analyze the results obtained from the experimental campaign, the heat pump model was utilized to determine the refrigerant charge required for each specific operating condition. Table 6 presents the inputs used and the corresponding calculated refrigerant charge. Although the calculated charge requirements are different depending on the conditions, the unit is charged with a fixed amount, as explained above.

Fig. 3 shows the schematic diagram of the unit. It represents qualitatively where the liquid refrigerant charge accumulates and where is reduced in case of undercharge in cooling mode for the conditions A35W7-30rps and A23W18-80rps. In addition, Fig. 4 shows the experimental measurements of SC and SH, and the residuals of the experimental measurements of the condensing temperature (Tc), evaporating temperature (Te), compressor discharge temperature (Tdis), and compressor power input (Wcomp) with different refrigerant charge levels and for the three cooling mode conditions tested. The A35W7-30rps condition requires less refrigerant charge compared to the others analyzed. This fact is related to the SC control implemented for this point to keep the water at temperatures higher than 0 °C and prevent freezing. The refrigerant charge in the system will mostly accumulate in the liquid state in the accumulator (as shown in Fig. 3a) with these control conditions and will not participate actively in the refrigeration cycle. A refrigerant leakage with values up to 85% will reduce the amount of refrigerant in the accumulator, but the SC control (as shown in Fig. 4a) will remain at the same values. However, following Fig. 4(b), if the refrigerant charge from this limit of 85% of the nominal, it is observed that the measured SH increases by approximately 6 K. This indicates that the accumulator is empty at this level and the system can no longer maintain saturation conditions at the outlet without SH. In the case of OC of 110%, there are no differences in SC and SH since the accumulator will have a higher level of refrigerant charge, but this will not affect these variables.

Fig. 4(c) shows the residual of Tc and 4(d) of Te. This condition (A35W7-30rps) has no changes on them with UC of 85% or OC of 110%. Fig. 4(e) shows the residual of Tdis, indicating an increase as the refrigerant charge decreases. This is due to the fact that when the level of liquid refrigerant in the accumulator is decreased, it enters the compressor with a higher vapor quality, resulting in a higher Tdis. Fig. 4(f) displays the residual of Wcomp, which is not affected by UC or OC at the imposed levels.

Fig. 3(b) indicates qualitatively the liquid refrigerant charge accumulation in the A23W18-80rps condition, which requires 0.72 kg. This condition's objective is to maintain the target SH at 5K, resulting in an almost empty accumulator at the evaporator's outlet. The refrigerant in liquid form will accumulate at the condenser's outlet, specifically the finned-tube in cooling mode. The SC value measured under these conditions is quite high (14.5K) since most of the liquid refrigerant is accumulated there. If the system has a refrigerant leakage or undercharging of 85%, the charge will decrease from the condenser outlet, leading to a decrease in SC (Fig. 4(a). However, Fig. 4(b) demonstrates that the SH can still be controlled, even if the refrigerant charge increases or decreases to those levels. The condition A35W18-60rps performance is equivalent, as the control and required charge are similar.

For these two conditions that have similar performance, Fig. 4(c) shows the residual of Tc, which increases with the refrigerant charge as in this case, the Tc is also bounded to subcooling values. Fig. 4(d) shows the residuals of Te, which remain unchanged with both UC and OC for these conditions. Furthermore, Fig. 4(e) demonstrates that the residual of Tdis almost does not vary with the charge since changes in this variable are related to the level of charge in the accumulator at the suction of the compressor. In these conditions, the accumulator is empty due to the control of a given SH of 5–7 K, which can keep control independently of the levels of refrigerant charge imposed. Fig. 4(f) shows that the Wcomp residual shows a slight variation for these conditions, mostly associated with the observed changes in the condenser pressure. The results obtained with the two conditions with

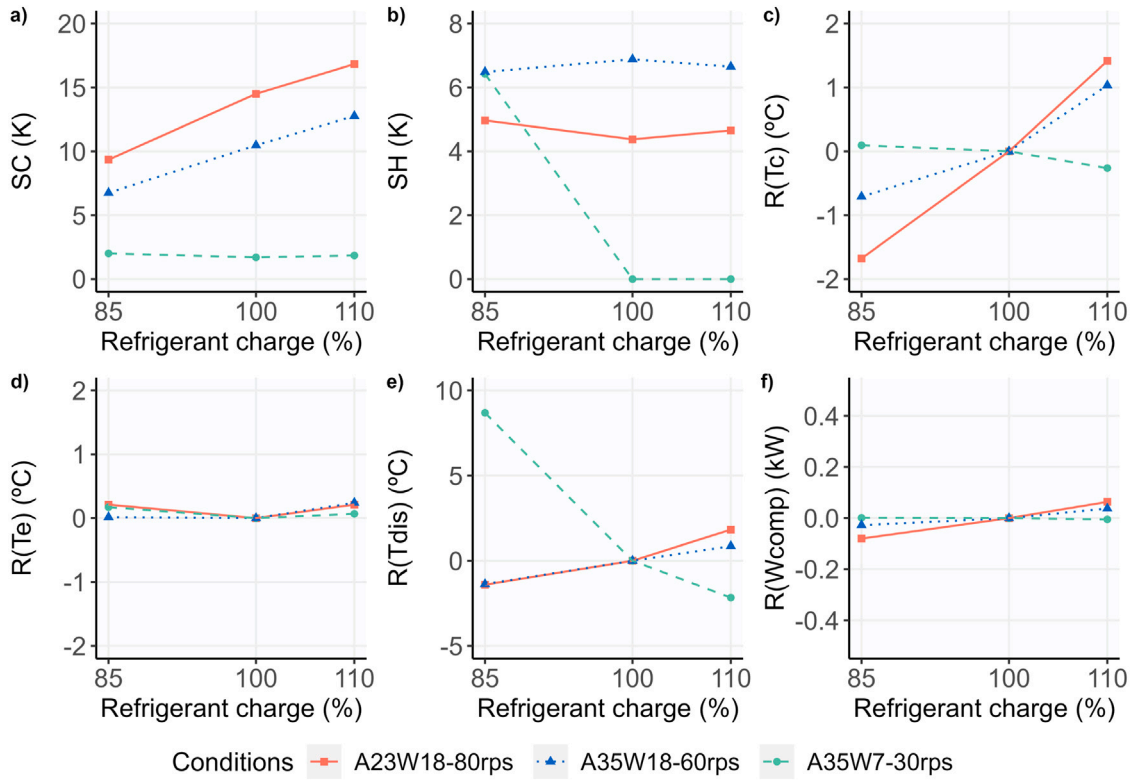

Fig. 4. Experimental measurements of (a) SC and (b) SH, and the residuals of the experimental measurements of (c) Tc, (d) Te, (e) Tdis, and (f) Wcomp with different refrigerant charge levels for three cooling mode conditions.

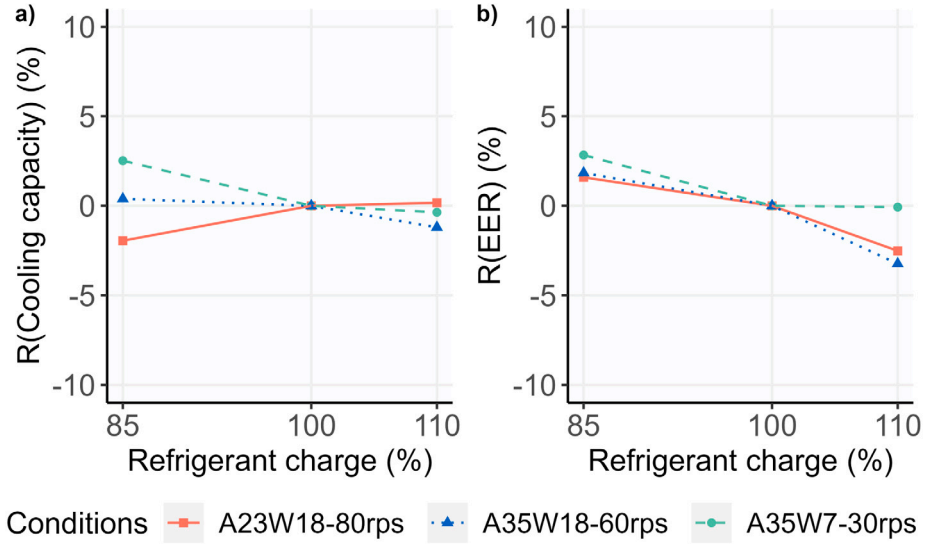

Fig. 5. Impact of undercharge (85%) and overcharge (110%) from experimental measurements, represented as a residual of (a) Cooling capacity and (b) EER for three cooling mode conditions.

SH control are similar to most of the related works from literature where UC and OC have been experimentally imposed (as shown in [7] or [9]). The heat pump's performance when varying the charge has a similar pattern when there is an expansion valve that controls SH and the accumulator is not used (when decreasing the charge, decreasing SC and Tc and, if the valve can still control, maintaining Te and SH).

Fig. 5 shows the impact of UC and OC in the three cooling mode conditions tested, represented with the residuals of cooling capacity and EER. The EER has been calculated as follows:

$$EER = \frac{Q_{evap}}{W_{total}} \quad (2)$$

Where Q_{evap} is the cooling capacity (capacity at the evaporator) and W_{total} is the total power input (including compressor, fan, and water pump). EER and cooling capacity residuals have been calculated as the percentage that varies with respect to the state of that fault-free condition to account for the impact on performance.

The most notable impact in the capacity occurs for the A23W18-80rps and 85% UC condition. It is reduced by 2%, mainly due to decreased liquid refrigerant at the condenser outlet. Even though the condition A35W18-60rps behaves similarly, the evolution of Tc and SC showed that these variables decreased to a lesser extent with the refrigerant charge with the condition A35W18-60rps, so it reduces less

Table 7
Refrigerant charge required at each tested operating point of the heating mode (calculated with the model).

Test condition	Water inlet T (°C)	Water outlet T (°C)	Evaporator inlet T (°C) and RH (%)	Airflow (m3/h)	Compressor Speed (rps)	SC (K)	SH (K)	Required charge (kg)
A2W35-35rps	32	35	2 (73%)	1977	35	6.5	0	1.01
A7W70-80rps	64	70	7 (88%)	1542	80	7.3	0	0.63
A10W45-80rps	38	45	10 (87%)	1402	80	9.7	0	0.68
A12W24-40rps	20	24	12 (88%)	1212	40	7.3	0	0.89

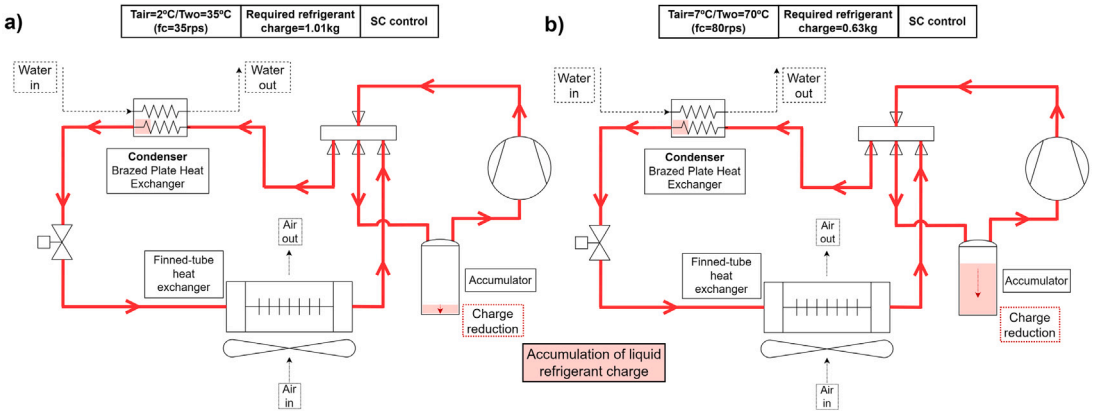

Fig. 6. Schematic diagram illustrating the liquid refrigerant charge accumulation and where it is reduced in case of undercharge in heating mode for conditions (a) A2W35-35rps and (b) A7W70-80rps.

the SC. It enters with lower quality to the evaporator, having thus less impact on capacity. Concerning the EER, the impact is not very noticeable for any condition. Despite the decrease in capacity with UC of A23W18-80rps, it does not impact the EER as it is compensated by a decrease in the consumption of the unit. The negative impact on EER of A23W18-80rps and A35W18-60rps with OC is due to the increase in consumption caused by the rise in condensing pressure. The A35W7-30rps condition has no impact on capacity and EER with the imposed UC and OC levels, mainly as a result of using the accumulator and SC control.

3.1.2. Heating mode

During heating mode, the EEV regulates the SC at the condenser outlet, regardless of the conditions. The SC target is based on a value that improves the system behavior based on reducing the discharge temperature and increasing the evaporating temperature. In this mode, the refrigerant in its liquid form will accumulate in the receiver at the evaporator outlet, which guarantees saturation conditions and a resulting SH of 0 K.

Similar to the analysis conducted for the cooling mode, Table 7 presents the inputs utilized and the corresponding calculated refrigerant charge for each heating mode condition with the heat pump model. Two conditions require more charge, specifically A2W35-35rps and A12W24-40rps, with the required refrigerant charge of 1.01 kg and 0.89 kg, respectively. The A7W70-80rps and A10W45-80rps conditions require less amount of refrigerant charge, with a quantity of 0.63 kg and 0.68 kg, respectively.

To evaluate the system's performance concerning different levels of refrigerant charge, an examination of certain variables has been conducted in two distinct conditions: A2W35-35rps, which requires the highest charge from the ones analyzed, and A7W70-80rps, which requires the least. Fig. 6 shows the schematic diagram of the unit, presenting qualitatively the liquid refrigerant charge accumulation and where it is reduced in case of undercharge in heating mode for the conditions A2W35-35rps and A7W70-80rps. Furthermore, Fig. 7 shows the experimental measurements of SC and SH, as well as the residuals of the experimental measurements of Tc, Te, Tdis, and Wcomp with different refrigerant charge levels for the four heating mode conditions tested.

Fig. 6(a) illustrates that the A2W35-35rps condition stores a smaller amount of liquid refrigerant charge in the accumulator at the evaporator outlet due to its higher charge demand. Consequently, any UC or refrigerant leakage event will result in a decrease in the liquid level of the accumulator. It is worth noting that A2W35-35rps requires a significant amount of refrigerant charge to function. With the refrigerant charge employed in the unit (the 100%), saturation conditions cannot be maintained at the outlet of the evaporator (i.e., the accumulator is with a low liquid level), and the SH is 5K instead of 0K as the rest of the conditions (Fig. 7b). This becomes more severe in the case of 85% of charge since a SH of 23K is achieved. Fig. 7(c) shows the residuals of Tc, that do not change with charge (the same way as SC keeps fixed). Nevertheless, Fig. 7(d) shows how Te drops in A2W35-35rps with UC of 85%, as the evaporating pressure decreases and the refrigerant enters with a higher quality to the evaporator. Fig. 7(e) shows that as the charge decreases, Tdis increases by reducing the level of the accumulator and increasing the SH, so the refrigerant enters the compressor with a lower vapor quality. In Fig. 7(f) can be observed that, when UC happens, although the evaporating pressure decreases and the compression ratio is higher, the refrigerant mass flow rate through the compressor also decreases, and the compressor consumption does not increase. An OC of 110% for this condition would ensure saturated conditions at the evaporator outlet and, therefore, SH of 0K. There is also a slight increase in Te and a decrease in Tdis, both due to the accumulator having a higher level. Similar conclusions can be applied to the results of A12W24-40rps since this condition also needs a high refrigerant charge. Nevertheless, the changes in the variables with charge are not so abrupt since the charge required is lower.

In the case of test condition A7W70-80rps, a lower amount of refrigerant charge is required compared to the previously described condition. Consequently, more liquid refrigerant will accumulate than in the previous case. The amount of refrigerant accumulated at the condenser outlet will depend on the value controlled by the EEV, which remains constant despite variations in the refrigerant charge (as shown in Fig. 7a). Fig. 6(b) represents qualitatively where the refrigerant charge in liquid state accumulates. Even reducing the charge to 85%, the level is sufficient to maintain saturation conditions at the outlet of the evaporator. To illustrate, Fig. 7(b) shows how the SH is kept at 0

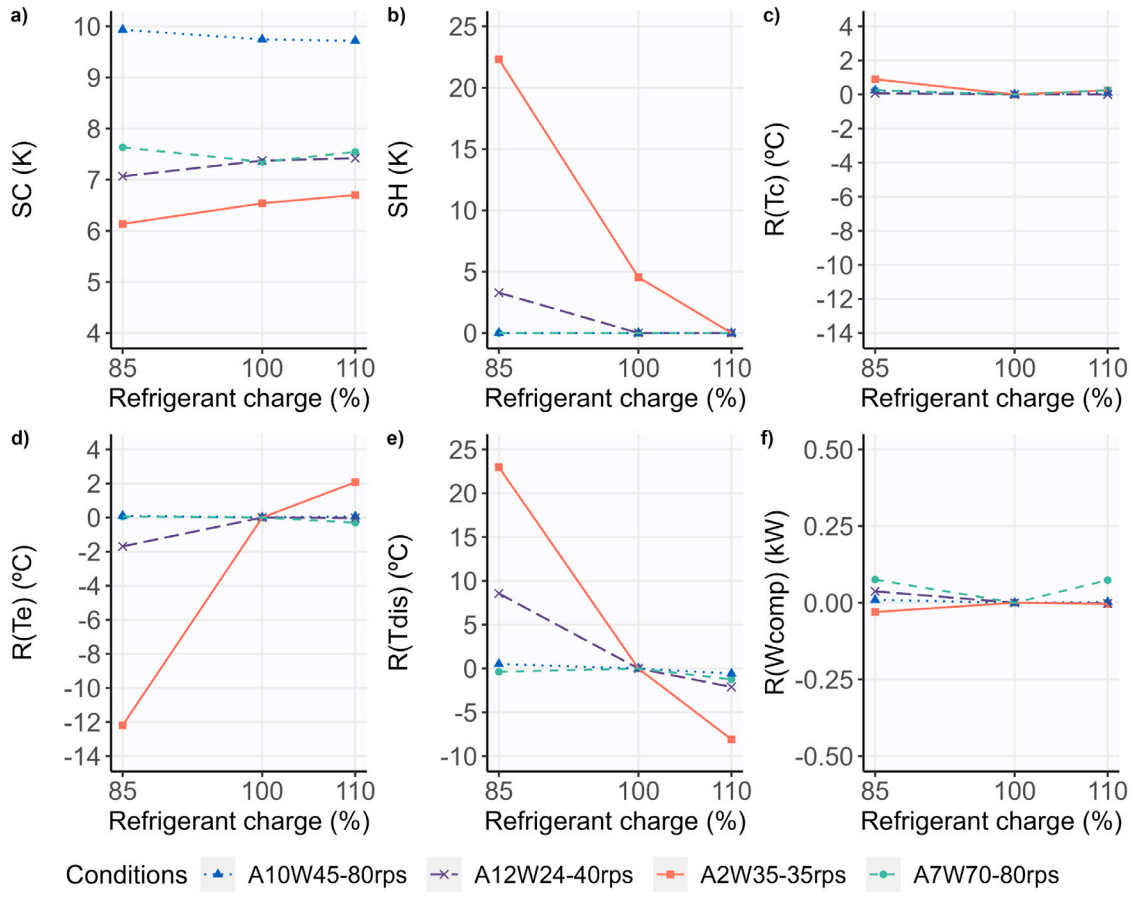

Fig. 7. Experimental measurements of (a) SC and (b) SH, and the residuals of the experimental measurements of (c) Tc, (d) Te, (e) Tdis, and (f) Wcomp with different refrigerant charge levels for four heating mode conditions.

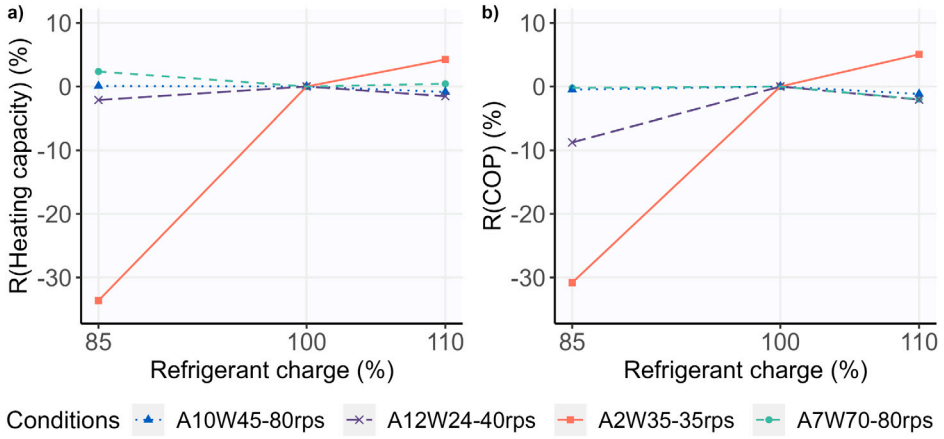

Fig. 8. Impact of undercharge (85%) and overcharge (110%) from experimental measurements, represented as a residual of (a) Heating capacity and (b) COP for four heating mode conditions.

K. Fig. 7 shows the residuals of (c) Tc, (d) Te, (e) Tdis, and (f) Wcomp with UC and OC. None of these variables shows significant changes with this condition since the accumulator in the suction maintains these levels of refrigerant charge imposed at an adequate level to continue operating with any observable changes. The A10W45-80rps condition operates similarly to A7W70-80rps, as it requires a comparable level of refrigerant charge.

Fig. 8 shows the impact of UC and OC in the four heating mode conditions tested, represented with the residuals of heating capacity and COP. The COP has been calculated as follows:

$$COP = \frac{Q_{cond}}{W_{total}} \tag{3}$$

Where Q_{cond} is the heating capacity (capacity at the condenser) and W_{total} is the total power input (including compressor, fan, and water pump). Similar to the cooling mode, COP and heating capacity residuals have been calculated as the percentage that varies with respect to the state of that fault-free condition to account for the impact on performance.

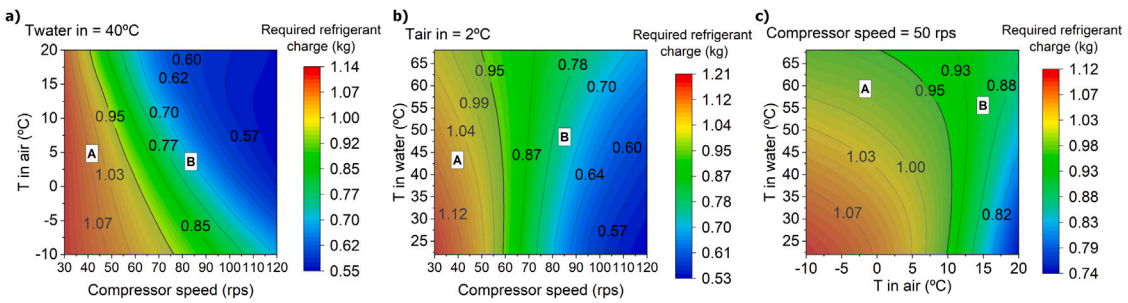

Fig. 9. Refrigerant charge required according to the working conditions of the unit in heating mode, setting in (a) T water in = 40 °C, (b) T air in = 2 °C, and (c) compressor speed = 50rps (calculated with the model).

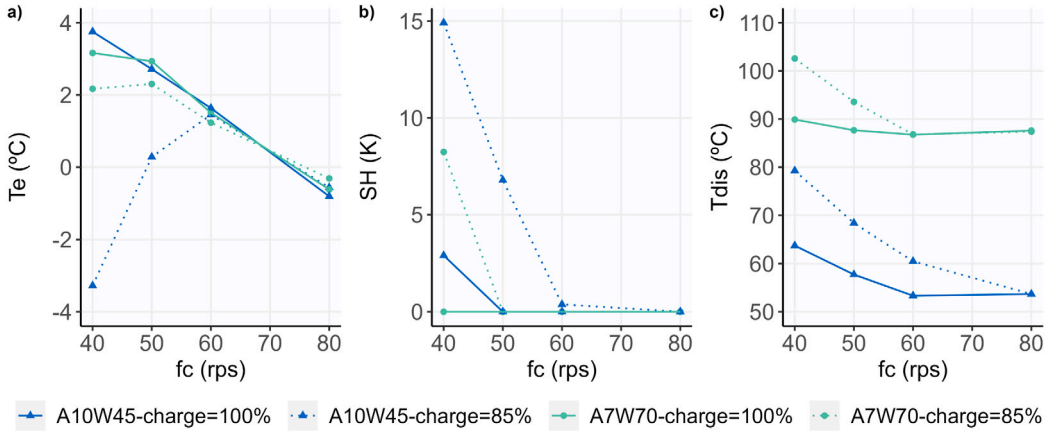

Fig. 10. Experimental measurements of (a) Te, (b) SH, and (c) Tdis varying the compressor speed with conditions A10W45 and A7W70 at 85% and 100% of the refrigerant charge.

It is observed that for conditions requiring less refrigerant charge (A10W45-80rps and A7W70-80rps), there is no influence in capacity or COP with the UC and OC levels imposed. However, A12W24-40rps and especially A2W35-35rps have a detrimental effect on capacity and noticeably on COP in the case of UC. This is mainly due to the reduction in mass flow rate with the drop in evaporating pressure when the refrigerant charge level in the accumulator is insufficient.

Expanding on the observed findings, it has been noticed that the variations in the analyzed system variables are dependent on the specific heating conditions. Thus, the amount of refrigerant charge needed under specific heating conditions plays a significant role in the detection of an undercharged event in this kind of system.

In order to learn more about how conditions affect the refrigerant charge requirements of the system, using the HP model presented before, a parametric analysis of the required refrigerant charge as a function of air and water temperatures and compressor speed conditions has been done. The results are presented in Figs. 9(a), 9(b), and 9(c). The figures can be divided into two zones based on the line representing the nominal charge of the system: *Zone A*, which requires a higher refrigerant charge and would have low refrigerant levels in the accumulator with 85% UC, leading to variations mainly in SH, Te, and Tdis; and *Zone B*, which requires less charge and would still maintain saturation conditions at the evaporator outlet even with 85% UC. The distinction between the two regions is based on the refrigerant charge at which changes in variables were observed experimentally during undercharge.

The performed analysis shows that the required refrigerant charge depends significantly on compressor speed for predefined external conditions, and based on that, that parameter can be used to identify charge problems in advance. Figs. 9(a) and 9(b) shows that phenomenon.

Experimental testing was conducted for conditions A10W45 and A7W70, where a compressor speed scanning (80, 60, 50, and 40 rps) was performed at 100% and 85% refrigerant charge levels. The results of (a) Te, (b) SH, and (c) Tdis for each compressor speed are shown in Fig. 10. It is observed that for the A10W45 condition, a speed of 50 rps causes it to shift from *Zone B* to *Zone A* due to significant differences in the three variables compared to 100% of charge. Similarly, for the A7W70 condition, a speed of 40 rps allows it to move to *Zone B* conditions, as there are significant differences in SH and Tdis with respect to 100% of refrigerant charge, indicating undercharging of the system.

3.2. Airflow restrictions

3.2.1. Cooling mode

In cooling mode, the fouling or airflow restrictions imposed on the finned-tube heat exchanger correspond to condenser fouling (CF). Fig. 11 shows the experimental measurements of SC and SH, and the residuals of the experimental measurements of Tc, Te, Tdis, and Wcomp with different CF levels for the three tested conditions. Figs. 11(a) and (b) illustrates how the different levels of CF affect SC and SH, respectively. At A23W18-80rps and A35W18-60rps conditions, EEV controls SH. This control remains effective with the increase of CF. However, SC increases as CF levels increase. On the other hand, at A35W7-30rps condition where SC is controlled, SC is maintained for all CF levels, as well as saturation conditions at the compressor suction can continue to be ensured by maintaining a SH of 0 K.

In Figs. 11(c), (d), (e), and (f), the main changes in the refrigerant cycle variables can be observed in the form of residuals. An increase in condenser fouling results in a decrease in the airflow rate, leading to an increase in Tc. As Tc rises and Te conditions remain unchanged, Tdis increases with the airflow rate reduction, resulting in an increase in Wcomp.

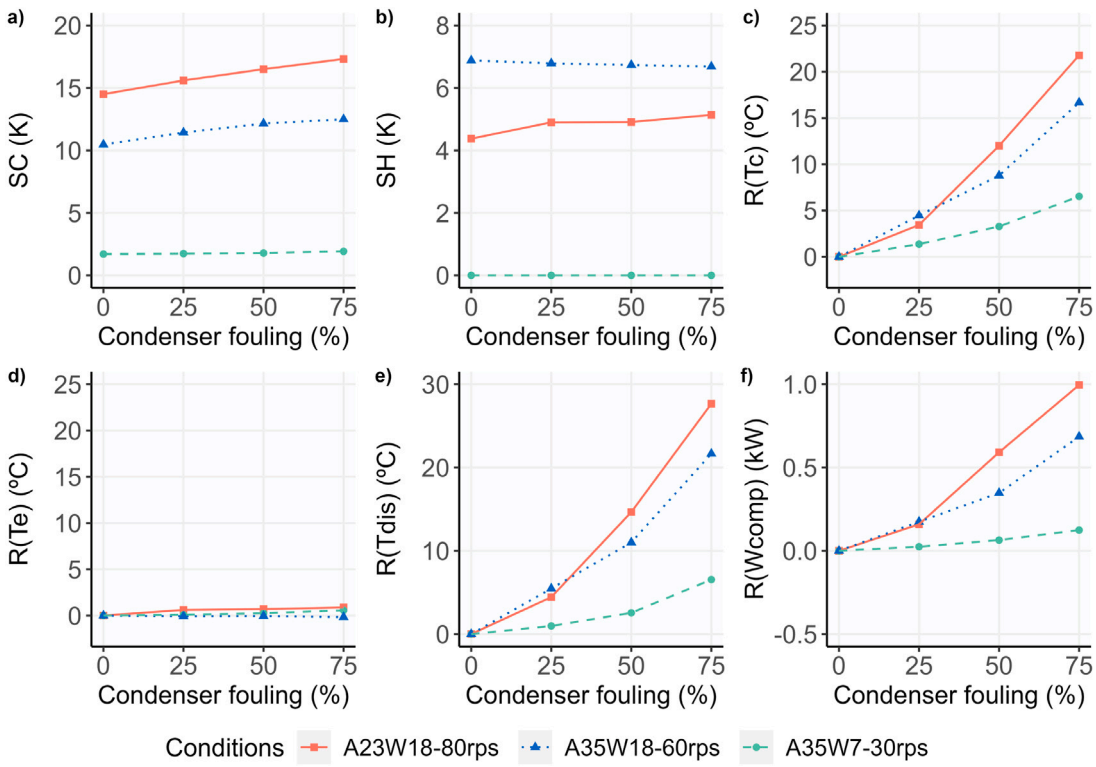

Fig. 11. Experimental measurements of (a) SC and (b) SH, and the residuals of the experimental measurements of (c) Tc, (d) Te, (d) Tdis, and (f) Wcomp with different condenser fouling levels for three cooling mode conditions.

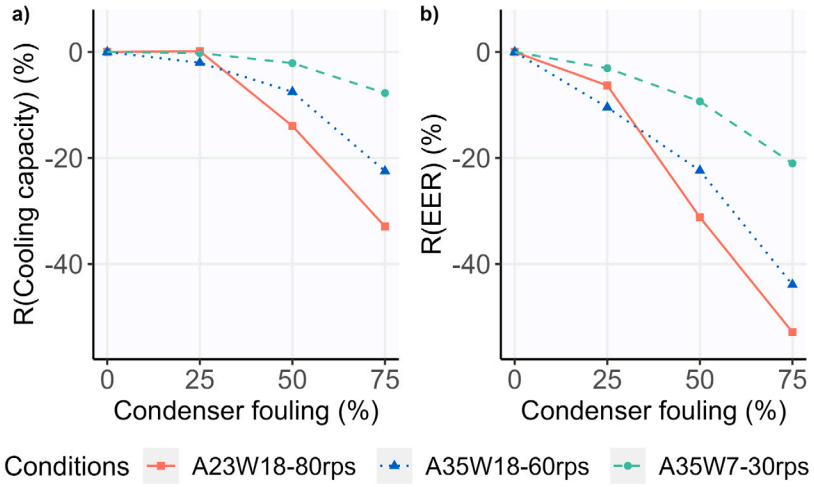

Fig. 12. Impact of condenser fouling from experimental measurements, represented as a residual of (a) Cooling capacity and (b) EER for three cooling mode conditions.

Fig. 12 shows the impact of CF in the three cooling mode conditions tested, represented with the residuals of cooling capacity and EER. The most notable variation in the capacity is for A23W18-80rps. It is reduced by almost 14% with 50% CF and 32% with 75% CF. It can also be seen that the effect of CF on EER is significant. As the CF level rises, both the capacity decreases, and Wcomp increases, leading to a significant reduction in EER. Besides, fouling has a higher impact on the system at higher values of compressor speed, as increasing the compressor speed increases the mass flow rate, and better heat transfer is required for the heat exchangers.

3.2.2. Heating mode

In heating mode, the fouling or airflow restrictions imposed on the finned-tube heat exchanger correspond to evaporator fouling (EF). Fig. 13 shows the experimental measurements of SC and SH, and the residuals of the experimental measurements of Tc, Te, Tdis, and Wcomp with different EF levels for the four tested conditions. Fig. 13(a) shows how the SC can be maintained despite increasing the EF level, except for the A10W45-80rps condition, where a slight decrease is observed. The SH, on the other hand, remains at 0 K due to the accumulator, except for A2W35-35rps (Fig. 13(b). In this condition, according to the previous Section 3.1.2, the system will require a higher refrigerant charge, and the level in the accumulator is too low to have saturated conditions.

The most significant variations in the refrigerant cycle are observed in Te since the airflow rate through the evaporator is reduced, and therefore Te decreases (Fig. 13(d). Tc is not affected for any level of EF or any of the conditions tested (Fig. 13(c). Additionally, the small

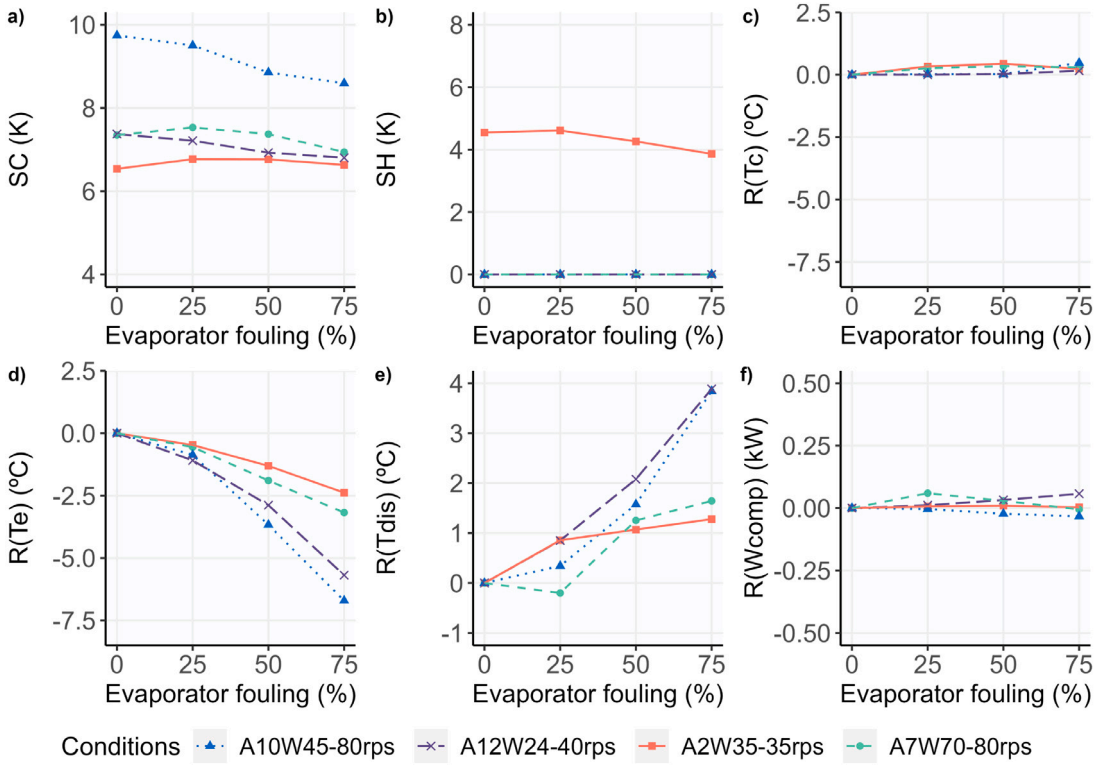

Fig. 13. Experimental measurements of (a) SC and (b) SH, and the residuals of the experimental measurements of (c)Tc, (d) Te, (e) Tdis, and (f) Wcomp with different evaporator fouling levels for four heating mode conditions.

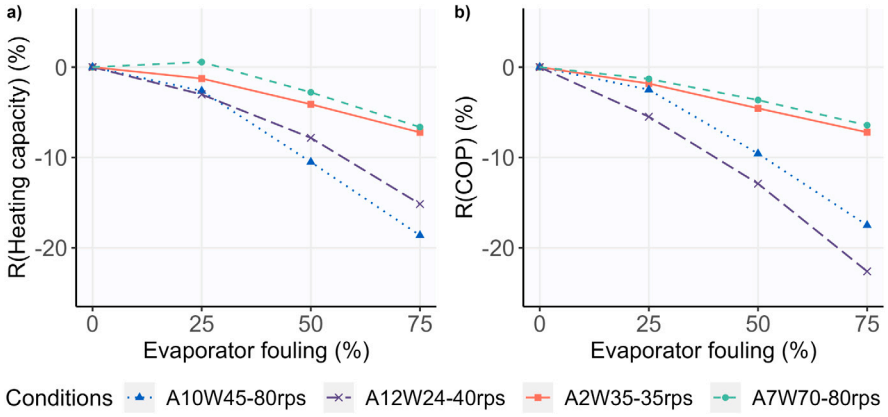

Fig. 14. Impact of evaporator fouling from experimental measurements, represented as a residual of (a) Heating capacity and (b) COP for four heating mode conditions.

changes in control by EEV in the SC might have influenced the compressor discharge temperature, which has been observed to decrease slightly as the EF level rises for some conditions. Fig. 13(e) shows these minor fluctuations in Tdis, which are not considered significant in the event of an EF fault. On the other hand, Wcomp remains unaffected in all scenarios and for all EF levels, as depicted in Fig. 13(f). Similar to the case with UC in heating, the evaporating pressure decreases, the compression ratio is higher, the refrigerant mass flow rate through the compressor also decreases, and Wcomp remains almost constant.

Fig. 14 shows the impact of EF in the four heating mode conditions tested, represented with the residuals of heating capacity and COP. The most notable capacity impact occurs for the A10W45-80rps. This is reduced by almost 20% with 75% EF. However, for the A2W35-35rps and A7W70-80rps conditions, capacity is less worsened with EF since they are the conditions where evaporation pressure drops the least as fouling increases. The effect of EF on the COP is noticeable, although to a lesser extent than in cooling mode. As the EF level rises, the capacity decreases, but the Wcomp remains practically the same, leading to a decrease in COP, but lower than in cooling. A12W24-40rps is affected more severely, with a 23% drop in COP at 75% EF. A7W70-80rps is less affected, as a 75% EF causes only a 6% drop in COP. As in cooling mode, when EF is at 25%, neither capacity nor COP is significantly impacted, and the unit's performance remains relatively unaffected.

It has thus been observed that, in cooling mode, Wcomp is significantly more affected than in heating mode since fouling affects Tc in cooling mode while in heating, it affects Te. According to the studies carried out in [33,34], this could be different if the unit used another type of compressor. These studies analyze the energy consumption and mass flow rate characteristics of scroll and reciprocating compressors. They conclude that the primary variable on which Wcomp depends in scroll compressors is the condensing pressure and point out that similar behavior is expected for rotary compressors like the one used in this HP. However, in reciprocating compressors, evaporating pressure will also

Table 8
Residuals of the experimental measurements of the selected variables and performance indicators with single and simultaneous UC, OC and CF for three conditions in the cooling mode. Shaded boxes indicate variables that change less than ±1.5 °C in the case of temperatures or temperature differences and ±10% in the case of other variables.

Variable	Conditions	UC 85%	OC 110%	CF 50%	UC 85% + CF 50%	OC 110% + CF 50%
R(Tc) (°C)	A23W18-80rps	−1.68	1.41	12.00	11.23	14.83
	A35W7-30rps	0.09	−0.26	3.28	3.66	3.06
	A35W18-60rps	−0.71	1.03	8.79	7.69	10.96
R(Te) (°C)	A23W18-80rps	0.21	0.21	0.70	0.26	0.79
	A35W7-30rps	0.17	0.07	0.25	0.17	0.30
	A35W18-60rps	0.02	0.24	−0.05	−0.14	1.00
R(SC) (K)	A23W18-80rps	−5.16	2.33	2.00	−4.19	5.62
	A35W7-30rps	0.31	0.15	0.08	0.35	0.23
	A35W18-60rps	−3.72	2.29	1.68	−2.86	5.03
R(SH) (K)	A23W18-80rps	0.59	0.28	0.53	0.50	0.50
	A35W7-30rps	6.42	0.00	0.00	6.48	0.00
	A35W18-60rps	−0.39	−0.23	−0.14	−0.41	0.06
R(Tdis) (°C)	A23W18-80rps	−1.41	1.83	14.65	13.95	18.40
	A35W7-30rps	8.68	−2.17	2.55	12.96	1.33
	A35W18-60rps	−1.37	0.86	11.00	9.29	13.47
R(Wcomp) (kW)	A23W18-80rps	−0.08	0.06	0.59	0.56	0.75
	A35W7-30rps	0.00	0.00	0.06	0.07	0.06
	A35W18-60rps	−0.03	0.04	0.35	0.30	0.44
R(mass flow rate) (kg/h)	A23W18-80rps	1.40	−1.00	−8.31	−17.93	−6.55
	A35W7-30rps	−0.63	−0.19	0.50	−1.28	0.44
	A35W18-60rps	3.93	−2.39	−0.13	−2.51	3.70
R(Cooling capacity) (%)	A23W18-80rps	−1.95	0.17	−13.97	−25.16	−12.37
	A35W7-30rps	2.52	−0.36	−2.11	−2.83	−1.96
	A35W18-60rps	0.39	−1.20	−7.53	−13.57	−2.16
R(EER) (%)	A23W18-80rps	1.59	−2.52	−31.22	−39.37	−33.59
	A35W7-30rps	2.84	−0.07	−9.33	−10.22	−8.79
	A35W18-60rps	1.83	−3.24	−22.40	−26.06	−21.45

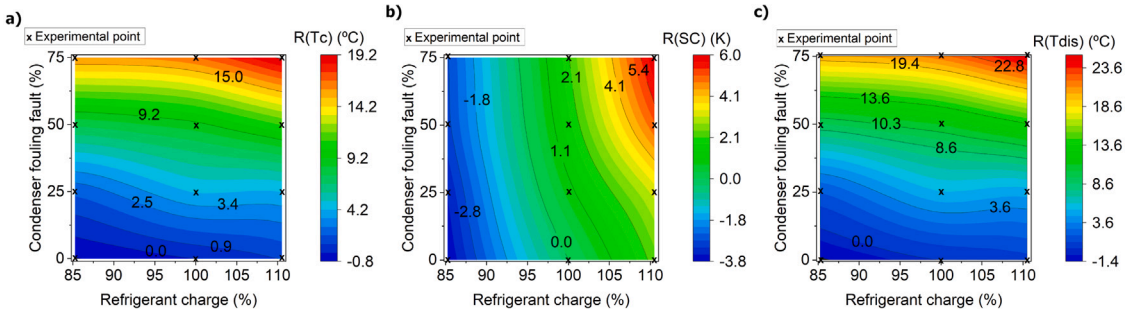

Fig. 15. Residuals of the experimental measurements of a) Tc, b) SC, and c) Tdis with simultaneous refrigerant charge and condenser fouling levels for the cooling mode condition A35W18-60rps.

have an influence, so employing it in the HP could lead to a different behavior in Wcomp than the one observed in this study.

Regarding the dependence of the influence on the compressor speed, as it increases, the faults associated with heat exchanger fouling have a higher impact on the system performance (taking into account the difference in temperature between the source and the sink, which affects the compression ratio and therefore the mass flow rate, having the opposite effect to the compressor speed). This trend generally follows the opposite direction from the one observed for UC faults, where they are more noticeable at lower speeds.

3.3. Simultaneous faults

3.3.1. Cooling mode

Fig. 15 shows the effects of the most relevant variables for the cooling mode using conditions A35W18-60rps as an example. It is important to note that the contour plots presented are derived exclusively from experimental data points indicated on the graphs. These plots represent the residuals of Tc, SC, and Tdis when UC/OC and CF occur simultaneously at different fault levels. Fig. 15(a) shows that Tc is much more sensitive to change with CF than with refrigerant charge variation. Fig. 15(b) demonstrates that refrigerant charge variation has a greater impact on SC in this mode. However, when CF (50%–75%) and OC are present at the same time, the SC increase is higher than when each fault is present individually. Tdis (Fig. 15c) varies similarly to Tc, i.e., with increasing CF, Tdis is also higher than when increasing the refrigerant charge. Notably, all three variables reach their maximum values when CF and OC co-occur.

Table 8 shows the residuals of the relevant variables in cooling mode for the three experimental tested operating conditions. In the case of UC/OC fault, the residuals for 85% UC and 110% OC are shown. In the case of fouling, the residuals for 50% CF are shown since it has been noted in previous sections that 25% CF has little impact on the system and 75% CF may be too unfavorable. For simultaneous double faults, they are shown combined with this level of 50% CF as well. Variables that do not change more than ±1.5 °C, if they are temperatures or temperature differences, have been shaded. The rest of the variables, if they do not change more than ±10%, have also

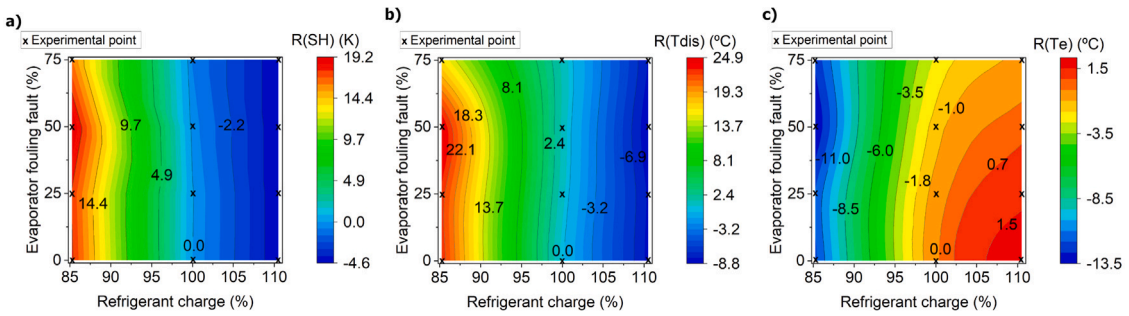

Fig. 16. Residuals of the experimental measurements of (a) SH, (b) Tdis, and (c) Te with simultaneous refrigerant charge and evaporator fouling levels for the heating mode condition A2W35-35rps.

Table 9
Residuals of the experimental measurements of the selected variables and performance indicators with single and simultaneous UC, OC and EF for four conditions in the heating mode. Shaded boxes indicate variables that change less than ±1.5 °C in the case of temperatures or temperature differences and ±10% in the case of other variables.

Variable	Conditions	UC 85%	OC 110%	EF 50%	UC 85% + EF 50%	OC 110% + EF 50%
R(Tc) (°C)	A2W35-35rps	0.90	0.25	0.44	0.42	0.16
	A7W70-80rps	0.26	0.26	0.34	0.59	0.43
	A10W45-80rps	0.24	0.09	0.02	0.01	−0.05
	A12W24-40rps	0.07	0.00	0.03	0.00	0.01
R(Te) (°C)	A2W35-35rps	−12.19	2.08	−1.31	−13.76	0.39
	A7W70-80rps	0.06	−0.30	−1.90	−1.57	−1.64
	A10W45-80rps	0.10	0.07	−3.67	−3.02	−2.64
	A12W24-40rps	−1.69	−0.02	−2.89	−3.92	−2.52
R(SC) (K)	A2W35-35rps	−0.40	0.16	0.23	0.01	−0.01
	A7W70-80rps	0.28	0.20	0.02	−0.01	−0.07
	A10W45-80rps	0.19	−0.03	−0.89	−0.61	−0.68
	A12W24-40rps	−0.31	0.05	−0.45	−0.29	−0.32
R(SH) (K)	A2W35-35rps	17.78	−4.55	−0.29	19.18	−4.55
	A7W70-80rps	0.00	0.00	0.00	0.00	0.00
	A10W45-80rps	0.00	0.00	0.00	0.00	0.00
	A12W24-40rps	3.29	0.00	0.00	3.30	0.00
R(Tdis) (°C)	A2W35-35rps	22.97	−8.10	1.07	24.85	−8.77
	A7W70-80rps	−0.37	−1.24	1.25	1.42	0.05
	A10W45-80rps	0.51	−0.58	1.57	1.58	0.53
	A12W24-40rps	8.56	−2.11	2.08	8.48	−1.82
R(Wcomp) (kW)	A2W35-35rps	−0.03	0.00	0.01	−0.03	0.00
	A7W70-80rps	0.08	0.07	0.03	0.05	0.05
	A10W45-80rps	0.01	0.00	−0.02	−0.02	−0.02
	A12W24-40rps	0.04	0.00	0.03	0.05	0.02
R(mass flow rate) (kg/h)	A2W35-35rps	−12.35	2.91	−1.34	−12.92	1.16
	A7W70-80rps	2.28	1.30	−2.73	−2.01	−2.08
	A10W45-80rps	0.00	−0.27	−9.40	−7.83	−7.15
	A12W24-40rps	−3.06	−0.17	−4.14	−6.15	−4.04
R(Heating capacity) (%)	A2W35-35rps	−33.63	4.25	−4.11	−35.42	−1.69
	A7W70-80rps	2.36	0.43	−2.79	−2.27	−3.12
	A10W45-80rps	0.07	−0.85	−10.50	−8.54	−8.25
	A12W24-40rps	−2.12	−1.53	−7.83	−8.82	−9.59
R(COP) (%)	A2W35-35rps	−30.82	5.05	−4.56	−32.21	−0.26
	A7W70-80rps	−0.21	−1.99	−3.64	−3.90	−4.61
	A10W45-80rps	−0.48	−1.17	−9.57	−7.86	−7.83
	A12W24-40rps	−8.76	−2.05	−12.89	−15.59	−14.16

been shaded. This table serves as a guide to know the variables that experience significant changes depending on the fault or combination of faults in this system. For instance, it is observed that in UC/OC faults, only the SC variable experiences considerable changes in conditions with SH control (A23W18-80rps and A35W18-60rps), and SH and Tdis for the condition with SC control (A35W7-30rps). In the case of CF or CF combined with UC or OC, the variables Tc, SC, Tdis, Wcomp, and mass flow rate may be significant in detecting the fault or combination of faults, depending on the condition.

3.3.2. Heating mode

The residuals of the most critical variables in heating mode (SH, Tdis, and Te) are presented in Fig. 16, using the example of condition A2W35-35rps. These contour plots have been elaborated from experimental tests with simultaneous fouling and UC/OC to illustrate the data. As explained in the previous sections, this condition requires a high refrigerant charge, and changes in SH, Te, and Tdis are observed when the charge is reduced and the accumulator liquid level decreases. The variables SH and Tdis (Figs. 16a and 16b) only change when the refrigerant charge is reduced, as adding the EF fault does not affect

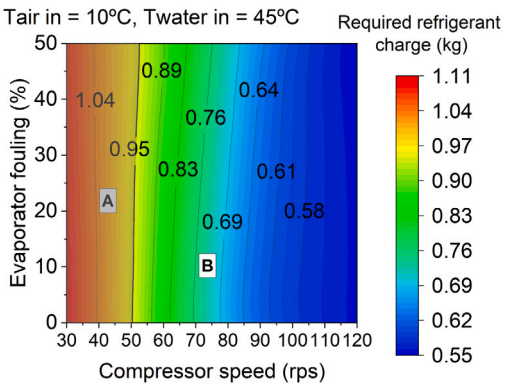

Fig. 17. Refrigerant charge required with conditions T air in = 10 °C and T water in = 45 °C, with different levels of Evaporator Fouling (%) and compressor speed (rps) (calculated with the model).

them. It is also noted that UC (85% charge) affects Te more than OC (110% charge). In the case of Te (Fig. 16c), reducing the refrigerant charge and increasing the EF fault results in a decrease of Te, although decreasing the charge has a more significant impact in this particular condition. Like SH and Tdis, the residuals of Te with OC are lower than those generated by an undercharged condition. On the other hand, contrary to the cooling mode, the variables Tc and SC do not vary practically in this mode when the two faults overlap, as they do not vary when the faults happen individually.

In addition, to expand the study explained in the previous section concerning how compressor speed affects the individual UC/OC fault, the heat pump model was used to analyze how compressor speed affects the fact of having a coupled fouling fault. For this purpose, a parametric study has been generated with different compressor speeds and EF levels (imposed in the model as reductions of the airflow with respect to the nominal, i.e., fouling of 20% is equivalent to 80% of the airflow that the fan should have through the evaporator). Fig. 17 shows in a contour plot the refrigerant charge required by the system by varying both the compressor speed and the EF levels, setting conditions of T air in = 10 °C and T water in = 45 °C. The separation between zone A (changes would be observed in variables SH, Te, and Tdis with 85% of UC) and zone B (less charge required and therefore saturation conditions would be maintained in the suction of the compressor with UC of 85%) has been marked. The study shows that the compressor speed is the variable with a higher influence on the charge requirement, and EF has a minimal impact on the required charge (as it has been seen that it mainly affects Te and the CHEX as the evaporator accumulates less charge than in cooling mode). Based on these results, the compressor speed can be integrated into the fault detection strategy for the UC as it does not have so much influence on EF.

The residuals of the relevant variables in heating mode for the four experimental tested operating conditions are displayed in Table 9. This table provides valuable insight into the variables that change in the event of UC, OC, EF, or a combination of these faults, similar to what has been described for the cooling mode. The unchanged variables are shaded for easy reference. Generally, for UC and OC faults, the variables Te, Tdis, and SH are useful in detecting it in conditions where a lot of refrigerant charge is needed and the accumulator level is low. Nevertheless, for the other conditions with a lower charge demand, this is not the case, as the accumulator ensures enough charge to operate even with UC. Reducing the compressor speed as part of the FDD can be helpful as it leads to a need for more refrigerant charge. As seen in previous sections, it results in a deviation from the expected value for Te, Tdis, and SH in case of UC fault. To detect EF, the variable Te can be used independently of the working condition, although it may vary more in some conditions than in others. For combined faults of UC+EF or OC+EF, Te, Tdis, and SH are the variables that undergo more changes, depending on the condition. To get a broader perspective, Table 9 can be consulted.

4. Conclusions

This study presents a comprehensive experimental analysis of a reversible air-to-water heat pump with undercharge, overcharge, and airflow restriction faults, both individually and in combination. The experimental tests have been carried out in cooling and heating modes. The effects on the main system variables and the impacts on performance have been analyzed, taking into account the type of control (SC or SH), the accumulator in the compressor suction, and the variable speed compressor. The key findings are:

- UC/OC faults:
  - In cooling mode with SH control, charge variation is primarily associated with SC variation for UC/OC faults.
  - With SC control, either in cooling or heating mode, OC leads to lower Tdis and higher Te, and UC results in higher Tdis, lower Te, and higher SH.
  - Low compressor speed necessitates a more effective charge, showing deviations in Tdis, SH, and Te under UC conditions. Modifying the compressor speed could thus be integrated into FDD techniques to identify refrigerant leaks, especially in systems with accumulators.
- Airflow Restrictions:
  - In cooling mode, airflow restrictions primarily affect SC, Tdis, and Tc, with greater impact under SH control than SC control.
  - In heating mode, the main impact of airflow restrictions is on Te.
  - Airflow restrictions significantly impact the EER in cooling mode due to increased Wcomp and decreased cooling capacity. In heating mode, the COP penalty is lower as Wcomp does not increase with fouling.
  - Higher compressor speeds amplify the impact of heat exchanger fouling on system performance.
- Combined UC/OC and airflow restrictions:
  - In cooling mode, the combination of OC and airflow restriction (CF) has a more significant impact on Tc, Tdis, and SC than when they occur individually.
  - In heating mode, the combined effect of UC or OC with airflow restriction (EF) is weaker compared to cooling mode, likely due to the higher charge in the CHEX in cooling mode.

This work has shown how challenging it can be when coupled faults occur because there can be overlapping effects on some variables. However, it has been seen that this can be affected by external parameters that can be controlled, such as compressor speed. Incorporating it into FDD methodologies presents a promising route for future exploration, given its demonstrated potential in this study. This can lead to the usage of other parameters, such as fan speed and EEV opening, when developing operation FDD algorithms. The value of this research is thus twofold: it deepens the understanding of residential air-to-water heat pump operation under soft faults and introduces the path for more sophisticated and effective diagnostic tools in heat pumps.

Declaration of competing interest

The authors declare that they have no known competing financial interests or personal relationships that could have appeared to influence the work reported in this paper.

Data availability

Data will be made available on request.

Acknowledgments

We gratefully acknowledge the financial support provided by the project "Decarbonización de edificios e industrias con sistemas híbridos de bomba de calor", funded by "Ministerio de Ciencia e Innovación" of Spain, with project code: PID2020-115665RB-I00. Belén Llopis-Mengual extends her appreciation to the Ministry of Universities of Spain through the "Formación de Profesorado Universitario" programme ref. FPU 19/04012.

References

[1] Eurostat, Energy Consumption in Households, Technical Report, 2021.
[2] European Heat Pump Association (EHPA), European Heat Pump Market and Statistics Report 2023, Technical Report, 2023.
[3] A.P. Rogers, F. Guo, B.P. Rasmussen, A review of fault detection and diagnosis methods for residential air conditioning systems, Build. Environ. (2019).
[4] Piotr A. Domanski, Hugh I. Henderson, W. Vance Payne, Sensitivity Analysis of Installation Faults on Heat Pump Performance, NIST Technical Note 1848, National Institute of Standards and Technology, Gaithersburg, MD, 2014.
[5] Alfonso William Mauro, Francesco Pelella, Luca Viscito, Performance degradation of air source heat pumps under faulty conditions, Case Stud. Therm. Eng. 45 (March) (2023) 103010.
[6] Larry Palmiter, Jun-Hyeung Kim, Ben Larson, Paul W. Francisco, Eckhard A. Groll, James E. Braun, Measured effect of airflow and refrigerant charge on the seasonal performance of an air-source heat pump using R-410A, Energy Build. 43 (7) (2011) 1802–1810.
[7] Zhimin Du, Piotr A. Domanski, W. Vance Payne, Effect of common faults on the performance of different types of vapor compression systems, Appl. Therm. Eng. 98 (2016) 61–72.
[8] Mehdi Mehrabi, David Yuill, Generalized effects of faults on normalized performance variables of air conditioners and heat pumps, Int. J. Refrig. 85 (2018) 409–430.
[9] Mehdi Mehrabi, David Yuill, Generalized effects of refrigerant charge on normalized performance variables of air conditioners and heat pumps, Int. J. Refrig. 76 (2017) 367–384.
[10] Woohyun Kim, Je-Hyeon Lee, Fault detection and diagnostics analysis of air conditioners using virtual sensors, Appl. Therm. Eng. 191 (2021) 116848.
[11] Seok Ho Yoon, W. Vance Payne, Piotr A. Domanski, Residential heat pump heating performance with single faults imposed, Appl. Therm. Eng. 31 (5) (2011) 765–771.
[12] Yifeng Hu, David P. Yuill, Amir Ebrahimifakhar, Ali Rooholghodos, An experimental study of the behavior of a high efficiency residential heat pump in cooling mode with common installation faults imposed, Appl. Therm. Eng. 184 (July 2020) (2021) 116116.
[13] Yifeng Hu, David P. Yuill, Seyed Ali Rooholghodos, Amir Ebrahimifakhar, Yuxuan Chen, Impacts of simultaneous operating faults on cooling performance of a high efficiency residential heat pump, Energy Build. 242 (2021) 110975.
[14] Yifeng Hu, David P. Yuill, Effects of multiple simultaneous faults on characteristic fault detection features of a heat pump in cooling mode, Energy Build. 251 (2021) 111355.
[15] Minsung Kim, Min Soo Kim, Performance investigation of a variable speed vapor compression system for fault detection and diagnosis, Int. J. Refrig. 28 (4) (2005) 481–488.
[16] I. Bellanco, F. Belío, M. Vallés, R. Gerber, J. Salom, Common fault effects on a natural refrigerant, variable-speed heat pump, Int. J. Refrig. (2021).
[17] Yabin Guo, Guannan Li, Huanxin Chen, Jiangyu Wang, Mengru Guo, Shaobo Sun, Wenju Hu, Optimized neural network-based fault diagnosis strategy for VRF system in heating mode using data mining, Appl. Therm. Eng. 125 (2017) 1402–1413.
[18] Derek Noël, Philippe Riviere, Dominique Marchio, Non-intrusive performance assessment method for heat pumps: Experimental validation and robustness evaluation facing faults, in: International Refrigeration and Air Conditioning Conference, 2018.
[19] Costantino Guzzardi, Marco Azzolin, Sandro Lazzarato, Davide Del Col, Refrigerant mass distribution in an invertible air-to-water heat pump: effect of the airflow velocity, Int. J. Refrig. 138 (2022) 180–196.
[20] Bruno Yuji Kimura De Carvalho, Pega Hrnjak, Evaluation Of Subcooling Control In Residential Heat Pumps Through Experimental And Model Analysis, in: International Refrigeration and Air Conditioning Conference, 2022.
[21] Bruno Yuji, Kimura De Carvalho, Pega Hrnjak, Experimental and theoretical analysis of subcooling control in residential air conditioning systems, in: International Refrigeration and Air Conditioning Conference, Purdue University, 2020.
[22] Bruno Yuji Kimura De Carvalho, Pega Hrnjak, Effect of Subcooling Control on Residential Heat Pump Systems' Performance, in: International Refrigeration and Air Conditioning Conference, Purdue University, 2020.
[23] Miquel Pitarch, Estefanía Hervas-Blasco, Emilio Navarro-Peris, José González-Maciá, José M. Corberán, Evaluation of optimal subcooling in subcritical heat pump systems, Int. J. Refrig. 78 (2017) 18–31.
[24] Estefanía Hervas-Blasco, Miquel Pitarch, Emilio Navarro-Peris, José M. Corberán, Study of different subcooling control strategies in order to enhance the performance of a heat pump, Int. J. Refrig. 88 (2018) 324–336.
[25] José M. Corberán, José González-Maciá, Pablo Montes, Rafael Blasco, 'ART', a computer code to assist the design of refrigeration and air conditioning equipment, in: International Refrigeration and Air Conditioning Conference, 2002.
[26] José M. Corberán, Pedro Fernández De Córdoba, José Gonzálvez, Francisco Alias, Semiexplicit method for wall temperature linked equations (SEWTLE): A general finite-volume technique for the calculation of complex heat exchangers, Numer. Heat Transfer B 40 (1) (2001) 37–59.
[27] E.W. Lemmon, I.H. Bell, M.L. Huber, M.O. McLinden, NIST standard reference database 23: Reference fluid thermodynamic and transport properties-REFPROP, version 10.0, national institute of standards and technology, 2018, http://dx.doi.org/10.18434/T4/1502528.
[28] José M. Corberán, Israel Martínez-Galván, Santiago Martínez-Ballester, José Gonzálvez-Maciá, Rafael Royo-Pastor, Influence of the source and sink temperatures on the optimal refrigerant charge of a water-to-water heat pump, Int. J. Refrig. 34 (4) (2011) 881–892.
[29] Miquel Pitarch, Emilio Navarro-Peris, José González-Maciá, José M. Corberán, Evaluation of different heat pump systems for sanitary hot water production using natural refrigerants, Appl. Energy 190 (2017) 911–919.
[30] J.R. García-Cascales, F. Vera-García, J.M. Corberán-Salvador, J. González-Maciá, Assessment of boiling and condensation heat transfer correlations in the modelling of plate heat exchangers, Int. J. Refrig. 30 (6) (2007) 1029–1041.
[31] Abdelrahman H. Hassan, José M. Corberán, Miguel Ramirez, Felipe Trebilcock-Kelly, Jorge Payá, A high-temperature heat pump for compressed heat energy storage applications: Design, modeling, and performance, Energy Rep. 8 (2022) 10833–10848.
[32] Belén Llopis-Mengual, Emilio Navarro-Peris, Selection of relevant features to detect and diagnose single and multiple simultaneous soft faults in air-source heat pumps, Appl. Therm. Eng. 238 (2024) 121922.
[33] Javier Marchante-Avellaneda, Jose M. Corberan, Emilio Navarro-Peris, Som S. Shrestha, Analysis of map-based models for reciprocating compressors and optimum selection of rating points, Int. J. Refrig. 153 (2023) 168–183, https://doi.org/10.1016/j.ijrefrig.2023.06.002.
[34] Javier Marchante-Avellaneda, Jose M. Corberan, Emilio Navarro-Peris, Som S. Shrestha, A critical analysis of the AHRI polynomials for scroll compressor characterization, Appl. Therm. Eng. 219 (2023) 119432.